

A coupled fiber-matrix model demonstrates highly inhomogeneous microstructural interactions in soft tissues under tensile load

Lijuan Zhang¹, Spencer P. Lake², Victor K. Lai³, Catalin R. Picu^{1,4}, Victor H. Barocas², Mark S. Shephard¹

¹Scientific Computation Research Center
Rensselaer Polytechnic Institute
Low Center for Industrial Innovation, CII-4011
110 8th Street
Troy, NY 12180

²Department of Biomedical Engineering
University of Minnesota
7-105 Nils Hasselmo Hall
312 Church Street SE
Minneapolis, MN 55455

³Department of Chemical Engineering and Materials Science
University of Minnesota
421 Washington Ave SE
Minneapolis, MN 55455

⁴Department of Mechanical, Aerospace and Nuclear Engineering
Rensselaer Polytechnic Institute
Jonsson Engineering Center Rm. 2049
110 8th Street
Troy, NY 12180

Keywords: computational biomechanics, collagen network, non-fibrillar matrix, fiber-matrix interaction, nonaffine behavior, soft tissue

Submitted to: Journal of Biomechanical Engineering

Corresponding Author:

Mark S. Shephard
Scientific Computation Research Center
Rensselaer Polytechnic Institute
Troy, NY 12180-3590
Ph: 518-276-6795
Fx: 518-276-4886
Email: shephard@rpi.edu

Abstract: A soft tissue's macroscopic behavior is largely determined by its microstructural components (often a collagen fiber network surrounded by a non-fibrillar matrix (NFM)). In the present study, a coupled fiber-matrix model was developed to quantify fully the internal stress field within such a tissue and to explore interactions between the collagen fiber network and non-fibrillar matrix (NFM). Voronoi tessellations (representing collagen networks) were embedded in a continuous three-dimensional NFM. Fibers were represented as one-dimensional nonlinear springs and the NFM, meshed via tetrahedra, was modeled as a compressible neo-Hookean solid. Multi-dimensional finite element modeling was employed to couple the two tissue components, and uniaxial tension was applied to the composite RVE. In terms of the overall RVE response (average stress, fiber orientation, Poisson's ratio), the coupled fiber-matrix model yielded results consistent with those obtained using a previously developed parallel model based upon superposition. The detailed stress field in the composite RVE demonstrated the high degree of inhomogeneity in NFM mechanics, which cannot be addressed by a parallel model. Distributions of maximum/minimum principal stresses in the NFM showed a transition from fiber-dominated to matrix-dominated behavior as the matrix shear modulus increased. The matrix-dominated behavior also included a shift in the fiber kinematics toward the affine limit. We conclude that if only gross averaged parameters are of interest, parallel-type models are suitable. If, however, one is concerned with phenomena, such as individual cell-fiber interactions or tissue failure, that could be altered by local variations in the stress field, then the detailed model is necessary in spite of its higher computational cost.

Introduction

The mechanical properties of many soft connective tissues are governed by a fiber network (primarily collagen in most tissues) and surrounding non-fibrillar matrix (NFM; e.g., proteoglycans, glycoaminoglycans, cells, etc.). To understand how healthy tissues function, and how properties change in injury and disease, it is necessary to quantify the mechanical response of both the collagen network and the NFM, as well as the nature of the interaction between these tissue constituents. Because the relative contribution of different tissue components is difficult to ascertain experimentally, mathematical modeling is frequently applied to empirical data to characterize and quantify the roles of collagen and NFM in imparting mechanical properties to soft tissues. Phenomenological models (e.g., [1-3]) provided initial insights into the mechanics of fibrillar tissues, and, more recently, structural models (e.g., [4-12]) have emerged that capture more information about the tissue architecture. With the collagen network thus defined, the NFM is often modeled using a simple mathematical representation, such as a neo-Hookean [13-16] or Mooney-Rivlin [17-20] solid, and assumed to contribute to the composite behavior in a summed or “parallel” sense. A limitation of this approach is the inability to evaluate local interactions between fibers and NFM. Some models have utilized an additional term to account for fiber-matrix interactions [18, 21-23], but in general, the appropriate definition for the interaction term is unknown. To overcome this limitation, the current study presents a method wherein the collagen fiber network and surrounding NFM are microscopically coupled, making it possible to evaluate specifically the interaction between fibers and matrix.

Recently, we developed a computational network-based microstructural model to examine how specific NFM properties alter the response of fiber-matrix composites under load [24]. This model, consisting of a representative volume element (RVE) containing a fiber network (collagen) and neo-Hookean solid (NFM), fit experimental data of collagen-agarose co-gels [25] well and provided insight into the role of NFM in tensile mechanics. The NFM was found to preserve volume and restrict collagen fiber reorganization in a concentration-dependent manner. Within a specific range of property values, the NFM pressurized the composite tissue in such a way as to result in a negative (compressive) stress in the loading direction, even though the RVE was loaded in tension. Although this model provided useful results, it was constructed according to the conventional “parallel” approach of superposition of the two constituents (i.e., collagen network and NFM), so it was unable to examine interactions between collagen fibers and the surrounding NFM (as mentioned above) or to identify inhomogeneities in the stress field. For example, in a uniaxial extension experiment, the average transverse and shear stresses would be zero, but local shear would surely occur in the neighborhood of a fiber. Such local stresses could be much larger than average values, which could have important implications in initiating failure of the NFM or in greatly altering the site-specific cellular environment. Therefore, the objective of this study was to develop a microstructural modeling approach capable of (a) quantifying local stresses throughout the computational domain and (b) exploring interactions between NFM and the embedded collagen network.

Methods

Modeling Approach. Large-network models (e.g., [26-31]) are composed of an arrangement of interconnected fibers, which are often represented as one-dimensional

linear springs or nonlinear rods. The NFM surrounds the fibers and permeates the non-fiber space in a fully three-dimensional manner. In order to couple these components in a unified scheme, a multi-dimensional modeling approach was employed. Such a formulation is advantageous in that the total number of degrees of freedom can be reduced without overall loss of accuracy. For example, collagen fibers can still be modeled as one-dimensional elements, thereby greatly reducing computational demand, while more detailed aspects of collagen fiber morphology (e.g., fiber crimp) can be taken into account mathematically (i.e., in the constitutive equation) instead of geometrically. A finite element mesh, constructed upon the framework of the fiber network, was then used to define the geometry of the NFM and to allow for coupled interactions between the NFM and specific fibers within the network. This study used a multidimensional meshing scheme to construct coupled representations of the collagen fiber network and the surrounding NFM in order to characterize the interactions between constituents in soft tissues subjected to tensile load. The newly developed *coupled* model was compared to our earlier *parallel* model [24].

Network Generation. Collagen gels were modeled using Voronoi networks [30] as described previously [24]. Seed points placed randomly within representative volume elements (RVEs) were used to construct Voronoi tessellations (Fig.1). After construction of the network, seed points were removed, and nodes were placed at the intersections of Voronoi edges with each other or with the RVE boundaries. Nodes were represented as freely rotating pin-joints. Initially isotropic networks were rescaled in the loading (x_1) direction and clipped to produce networks within a cubic domain whose alignment matched polarized light alignment data from collagen-agarose co-gel experiments [25].

Any isolated fibers or fiber clusters were removed to leave a single, fully interconnected network in each RVE. Five similar but distinct RVEs were created (Table 1) and analyzed. Collagen fibers were represented as one-dimensional nonlinear springs with constitutive behavior defined as [13, 28, 32]:

$$f = \frac{E_f A}{B} (e^{B\varepsilon} - 1) \quad (1)$$

where f is force in given fiber, E_f is fiber Young's modulus in the zero-strain limit, A is cross-sectional area, B is a nonlinearity constant, and ε is the fiber Green strain along the fiber. Equation 1 specified properties for individual fibers, but the mechanical response of each RVE resulted from the collective behavior of the full network of fibers. Fiber parameters (i.e., E_f , A , and B) were defined using values similar to those used previously [24, 28]. The NFM was represented as a compressible neo-Hookean solid, with the Cauchy stress defined as [33]:

$$\sigma_{ij}^{nfm} = G \left(\frac{F_{ik} F_{jk}}{J} - J^{-2\beta-1} \delta_{ij} \right) \quad (2)$$

where G is shear modulus, F is the deformation gradient tensor, J is the determinant of F , $\beta = \nu_{nfm}/(1-2\nu_{nfm})$, and ν_{nfm} is Poisson's ratio of the NFM. As done previously [34], ν_{nfm} was set to 0.1. The NFM shear modulus was varied over a range of values ($G = 10, 110, 720$ and 4300 Pa) corresponding to 0.05, 0.125, 0.25 and 0.5 % w/v agarose [35] in our experimental collagen-agarose studies [25, 36]. To assess the role of compressibility, a set of simulations with $\nu_{nfm}=0.45$ was also evaluated for $G=110$ Pa. Built upon this common framework, parallel and coupled models were evaluated for each network as described below.

Parallel Model. We previously [24] presented results from simulations using a

parallel fiber-matrix model. In the current study, results obtained from simulating a wider range of G values are presented. Some relevant details of the parallel model are repeated here for clarity, and to highlight differences between the parallel approach and the newly-developed coupled model (described below). In the parallel model, the stress due to the collagen network was computed via a volume-averaging approach [37, 38] based on the nodal forces on each RVE boundary:

$$\langle \sigma_{ij}^{col} \rangle = \frac{1}{V} \sum_{\substack{\text{boundary} \\ \text{nodes}}} x_i f_j \quad (3)$$

where V is RVE volume, and f_j are the forces acting on boundary nodes (at positions x_i). Neo-Hookean NFM stresses were dependent only on the macroscopic deformation of the RVE, and the two stress components were combined in a simple summed (parallel) sense:

$$\sigma^{tot} = \langle \sigma^{col} \rangle + \sigma^{nfm} \quad (4)$$

After application of RVE strain, positions of the internal nodes and of the unloaded boundaries were adjusted iteratively until the force balance at each internal node was satisfied and the total stresses on the free surfaces were minimized.

Coupled Model. A coupled fiber-matrix microstructural model was developed and used to model the interactions between collagen fibers and NFM. A geometric model of the RVE with the two constituents (i.e. collagen fibers and surrounding NFM) was represented as a 3D non-manifold geometric model [39] with the embedded fiber network treated as 1D wire edges. The work-flow of applying finite element method in the coupled model is shown in Fig. 2(a). The complete definition of a Voronoi fiber network including fiber connectivity (network topology) and crosslink coordinates (network shape) was provided by a fiber network generation module and then used as input for creating the multi-

dimensional non-manifold geometry via Parasolid API [40]. Simmetrix [41, 42] meshing tools were used to create the conforming mesh from the generated RVE geometry.

The generated mesh was multi-dimensional with 3D tetrahedra for the solid matrix and 1D truss elements for the collagen fibers. The solid matrix and embedded fiber network were meshed together such that mesh vertices and mesh edges on the fibers were shared with the adjacent 3D solid elements (Fig. 2(b)). Fig. 2(c) shows the interior of the mixed dimensional mesh with shapes of elements intersecting the cutting plane retained. Displacements (u_1 , u_2 , and u_3) were selected as the nodal variables, and linear shape functions were used to interpolate the displacement field. Since linear tetrahedral and truss elements have the same nodal displacement variable, consistency between the two different dimensional elements was ensured. Newton-Raphson iteration was used to solve the nonlinear finite element equations describing the mechanics of the coupled system.

Model Solution and Analysis. For the coupled model, 0.5% strain steps were applied incrementally in the 1-direction until an RVE strain of 10% was achieved (i.e., $\lambda_1^{max} = 1.1$). The parallel model simulations were evaluated at a single displacement step of 10% for comparison. For both models, simulations were under quasi-static conditions, and stress-free boundaries were maintained in the transverse 2- and 3-directions. The following output measures were evaluated:

- Normal Cauchy stress (σ_{11}) from fibers and NFM
- Apparent Poisson's ratio of the composite RVE (ν_{rve}) obtained by averaging the values in 1-2 and 1-3 directions:

$$\nu_{12} = -\frac{\ln\lambda_2}{\ln\lambda_1}, \quad \nu_{13} = -\frac{\ln\lambda_3}{\ln\lambda_1} \quad (5)$$

where λ_1 , λ_2 and λ_3 are stretch ratios in 1, 2 and 3 direction, respectively

- Average fiber stretch (λ_{fb})
- Fiber orientation measured using the axial component of the projected 2D orientation tensor, Ω_{11} :

$$\boldsymbol{\Omega} = \frac{\sum l_i \begin{bmatrix} \cos^2 \theta_i & \cos \theta_i \sin \theta_i \\ \cos \theta_i \sin \theta_i & \sin^2 \theta_i \end{bmatrix}}{\sum l_i}, \quad \Omega_{11} = \frac{\sum l_i \cos^2 \theta_i}{\sum l_i} \quad (6)$$

In addition, the coupled model was used to evaluate stress distributions (for the six unique components of the Cauchy stress tensor) on transverse slices through the RVE mid-section (i.e., in the 2-3 plane), as well as distributions of maximum and minimum principal stress and fiber stretch.

Results

In the coupled fiber-matrix model, stress due to the fiber network increased with increasing NFM shear modulus, and the non-linearity of fiber stress-strain curves became less pronounced at higher G values (Fig.3(a)). As one might expect, the matrix stress increased with increasing NFM shear modulus (Fig.3(b)), which accounted for much of the increase in total stress (Fig.3(c)). RVE Poisson's ratio decreased with increasing G , but increased with strain for $G=10$ and 110 Pa (Fig.3(d)). In addition to comparing model results computed at the same imposed strain, results were also evaluated at the same imposed total stress (in this case, 200 Pa). Matrix stress values increased with increasing shear modulus for both cases (Fig.4(a)). In contrast, fiber stress values increased for the constant strain case, but decreased for the constant total stress case (Fig.4(b)), with the stiffer NFM shielding the collagen network.

Results from the coupled model were similar to those from the parallel model. Specifically, parallel and coupled models produced nearly identical average matrix stress

values (Fig.5(a)). The coupled model exhibited smaller fiber stress values (Fig.5(b)), but both models showed similar fractions of total stress as a function of different G (Fig.5(c)). In both cases, when ν_{nfm} was increased from 0.1 to 0.45, a slight increase and decrease were seen in fiber and matrix stress, respectively, with no net change in total stress.

In addition to normal stresses in the loading direction, several other metrics were similar for the coupled and parallel models. Average fiber stretch increased with increasing G (Fig.6(a)), while ν_{rve} (Fig.6(b)) and fiber orientation (represented via Ω_{11} ; Fig.6(c)) both decreased with increasing G . For each of these output parameters, values were slightly smaller for the coupled model, but showed the same patterns of change as a function of shear modulus. At high NFM Poisson's ratio (i.e., $\nu_{nfm}=0.45$), λ_{fib} and ν_{rve} were slightly increased and decreased, respectively, with no change in Ω_{11} .

The use of the coupled model allowed for full-field quantification of the six independent Cauchy stress components of the matrix material, visualized via slice plots through the RVE midsection. Figure 7 shows representative plots for $G = 720$ Pa, where black dots represent intersection points between fibers and the cutting plane. Tensile normal stresses (i.e., positive values) were evident in the loading direction (σ_{11}), whereas compressive stresses were observed in the transverse axes (e.g., σ_{22} and σ_{33}) in response to the extreme tendency of the collagen network to contract in the unloaded directions. The stress distribution in the matrix material was highly inhomogeneous for all stress components. Normal stress values in the loading direction were smaller in the vicinity of multiple fiber intersection points. Stress concentrations (either positive or negative) occurred in locations where two or more fibers traversed the slice plane in close proximity.

The detailed mechanical response of the NFM in the coupled model was investigated by analyzing the distribution of maximum principal stresses (Fig.8(a)) and minimum principal stresses (Fig.8(b)) evaluated at the Gauss points of the matrix material mesh. As G increased, both the maximum and minimum principal stress distribution curves moved along the positive x -axis, indicating that more matrix elements experienced tension under applied stretch. The mean values of the distribution curves approached values corresponding to the affine model at higher G , along with decreasing spread (i.e., standard deviation). In the curve of minimum principal stress distribution (Fig.8(b)), nearly all values were negative, indicating that much of the NFM was in compression.

Distributions of fiber stretch values were plotted against varying shear modulus and compared to the affine model (Fig.9). For lower G values (i.e. $G=10\text{Pa}$ and 110Pa), a majority of fibers exhibited values of ~ 1 (i.e., unstretched). At higher shear modulus, fiber stretch values became more distributed, with a larger portion near the higher limit of the distribution, and demonstrated distributions that were increasingly similar to results from the affine model.

Discussion

A coupled fiber-matrix microstructural model was developed and utilized to explore the interactions between constituents in soft tissues subjected to tensile load. Specifically, Voronoi tessellations, representing collagen fiber networks, were embedded in a continuous non-fibrillar matrix, represented via tetrahedral finite elements, and coupled using a multi-dimensional mesh framework. In terms of the bulk properties and overall RVE response, the coupled model yielded results consistent with those obtained using a simplified parallel model (Figs.5 and 6) described previously [24]. Thus, for investigations

concerned only with average behavior, microstructural models that assume a superposition or rule-of-mixtures framework (e.g., [13, 14, 22-24, 27]) may be sufficient. In cases where additional detail regarding inhomogeneities in NFM mechanics and/or quantification of fiber-matrix interactions are desired, however, a fully coupled model, such as the one developed in this study, can provide insight that is not attainable using a parallel-type model.

In our previous study [24], a parallel fiber-matrix microstructural model was used to predict the mechanical response of collagen-agarose co-gels, which have been used as a simple experimental test system to quantify the contribution of non-fibrillar matrix to soft tissue properties [25, 36]. In the present work, we compared the detailed coupled model to that parallel model. Both models predicted qualitatively the composition-dependent mechanical response of collagen-agarose co-gels in tension. Matrix stress (Fig. 5(a)), total stress fraction (Fig.5(c)), fiber orientation (Fig. 6(c)), and Poisson's ratio values (Fig.6(b)) agreed particularly well between the two models, while the coupled model demonstrated slightly lower mean fiber stretch (Fig.6(a)) and fiber stress values (Fig. 5(b)) than the parallel model. This discrepancy could be due to a mechanism wherein the matrix material has a stronger stress shielding effect on the embedded collagen network in the coupled model than in the parallel model. The stress shielding effect is revealed in Fig.4(b), in which fiber stress decreased as matrix material stiffness increased at constant stress.

Results obtained via the coupled model for bulk RVE properties were generally as expected. Stress values increased with strain, and both fiber and matrix stresses at a given strain increased with NFM shear modulus (Fig.3). A nonlinear toe-region was observed in the fiber stress-strain curve at small NFM modulus values, but nonlinearity was less

pronounced at larger NFM modulus values. The tendency toward linearity is consistent with a stiffer NFM eliminating the non-affine, low-stretch reorientation of the fiber network (Fig.9). This difference in reorientation also explains the decreased lateral compaction, and hence Poisson's ratio, with increasing NFM stiffness. In addition, the nonlinear relationship of Poisson's ratio and strain at low G (Fig.3(d)) closely matched the relationship observed in experimental tests of collagen-agarose co-gels [25]. The bulk RVE stresses analyzed in this model were obtained from simulations at a constant strain value (e.g., 10% stretch). When results were computed at a constant total stress (200 Pa) for each of the varied simulations, fiber stresses decreased with increasing NFM modulus, demonstrating a stress shielding role of the NFM at large G .

A significant strength of the coupled model is its ability to quantify the internal RVE stress field and interaction between fiber and matrix materials. The embedded fiber network had a significant effect on the stress field of the surrounding matrix material, as demonstrated by the inhomogeneity of internal stress distribution (Fig. 7). Tensile normal stresses in the loading direction (σ_{11}) were relatively consistent across the RVEs, although smaller values were observed in the vicinity of multiple fiber intersection points. Compressive normal stresses in traverse directions (i.e., σ_{22} and σ_{33}) were caused by fibers squeezing the surrounding matrix material in the lateral direction during reorientation. Due to the Poisson effect, matrix material being compressed in the lateral directions was concurrently stretched in the loading direction, thereby decreasing the local tensile stress and leading to smaller σ_{11} values in areas of concentrated fiber intersection points. Finally, maps of internal shear stresses demonstrated complex patterns (Fig.7(bottom)), with areas of particularly high shear stress co-localized with significant fiber clustering.

A defining characteristic of large-network simulations, in which fibers function in a fully-interacting organizational structure, is non-affine fiber kinematics [26]. After incorporating matrix material with the fiber network in this coupled model, we investigated how the NFM altered the relative affinity of the materials in the composite RVE. Distributions of maximum/minimum principal stress of the matrix material normalized by NFM shear modulus showed a transition from non-affine to affine behavior as the modulus increased (Fig.8). With higher matrix stiffness the system became dominated by the NFM, with more matrix stress values approaching the affine case. In other words, as the shear modulus increased, the composite response transitioned from a fiber-dominated to a matrix-dominated response. The matrix material also altered the kinematics of the embedded fiber network (Fig.9). At low shear modulus, the NFM had less ability to prevent fibers from reorienting to the load direction, which resulted in minimal stretching of fibers as seen by the high frequency of fibers with low stretch values of ~ 1 . With smaller matrix stiffness, the energy minimization of the matrix-fiber system was achieved mainly through fiber reorientation, which requires less work than fiber stretching. As the matrix stiffened and became more dominant, the fibers tended to stretch with their surrounding matrix material, leading to a higher frequency of large fiber stretch values (i.e., $\lambda_{fib} > 1.05$).

In conclusion, by providing detailed descriptions of the inhomogeneities and direction-dependence of internal RVE stress fields, the fully-coupled model has many potential applications, such as quantifying the local environment of cells or examining microscale local failure of tissues by stress concentration. Compared to a parallel model framework, however, the coupled model is much more computationally expensive. Since

both of these models provide good predictions in terms of gross average parameters (e.g., fiber orientation parameter, averaged stresses, etc.), parallel-type models are suitable, and even preferable, if specific details on fiber-matrix interactions are not needed.

Acknowledgements

The authors gratefully acknowledge the financial support of the National Institutes of Health (R01-EB005813 and F32-EB012352) and the American Heart Association (11PRE5410003).

References

- [1] Fung, Y. C., 1967, "Elasticity of soft tissues in simple elongation," *Am J Physiol*, 213(6), pp. 1532-1544.
- [2] Humphrey, J. D., 1995, "Mechanics of the arterial wall: review and directions," *Crit Rev Biomed Eng*, 23(1-2), pp. 1-162.
- [3] Horgan, C. O., and Saccomandi, G., 2003, "A description of arterial wall mechanics using limiting chain extensibility constitutive models," *Biomech Model Mechanobiol*, 1(4), pp. 251-266.
- [4] Lanir, Y., 1979, "A structural theory for the homogeneous biaxial stress-strain relationships in flat collagenous tissues," *J Biomech*, 12(6), pp. 423-436.
- [5] Decraemer, W. F., Maes, M. A., and Vanhuyse, V. J., 1980, "An elastic stress-strain relation for soft biological tissues based on a structural model," *J Biomech*, 13(6), pp. 463-468.
- [6] Kwan, M. K., and Woo, S. L., 1989, "A structural model to describe the nonlinear stress-strain behavior for parallel-fibered collagenous tissues," *J Biomech Eng*, 111(4), pp. 361-363.
- [7] Cortes, D. H., Lake, S. P., Kadlowec, J. A., Soslowsky, L. J., and Elliott, D. M., 2010, "Characterizing the mechanical contribution of fiber angular distribution in connective tissue: comparison of two modeling approaches," *Biomech Model Mechanobiol*, 9(5), pp. 651-658.
- [8] Wagner, H. P., and Humphrey, J. D., 2011, "Differential passive and active biaxial mechanical behaviors of muscular and elastic arteries: basilar versus common carotid," *J Biomech Eng*, 133(5), p. 051009.
- [9] Hollander, Y., Durban, D., Lu, X., Kassab, G. S., and Lanir, Y., 2011, "Experimentally validated microstructural 3D constitutive model of coronary arterial media," *J Biomech Eng*, 133(3), p. 031007.
- [10] Kao, P. H., Lammers, S. R., Tian, L., Hunter, K., Stenmark, K. R., Shandas, R., and Qi, H. J., 2011, "A microstructurally driven model for pulmonary artery tissue," *J Biomech Eng*, 133(5), p. 051002.

- [11] Soares, A. L., Stekelenburg, M., and Baaijens, F. P., 2011, "Remodeling of the collagen fiber architecture due to compaction in small vessels under tissue engineered conditions," *J Biomech Eng*, 133(7), p. 071002.
- [12] Szczesny, S. E., Peloquin, J. M., Cortes, D. H., Kadlowec, J. A., Soslowsky, L. J., and Elliott, D. M., 2012, "Biaxial tensile testing and constitutive modeling of human supraspinatus tendon," *J Biomech Eng*, 134(2), p. 021004.
- [13] Holzapfel, G. A., Gasser, T. C., and Ogden, R. W., 2000, "A new constitutive framework for arterial wall mechanics and a comparative study of material models," *Journal of Elasticity*, 61, pp. 1-48.
- [14] Driessen, N. J., Bouten, C. V., and Baaijens, F. P., 2005, "A structural constitutive model for collagenous cardiovascular tissues incorporating the angular fiber distribution," *J Biomech Eng*, 127(3), pp. 494-503.
- [15] Tang, H., Buehler, M. J., and Moran, B., 2009, "A constitutive model of soft tissue: from nanoscale collagen to tissue continuum," *Ann Biomed Eng*, 37(6), pp. 1117-1130.
- [16] Nagel, T., and Kelly, D. J., 2012, "Remodelling of collagen fibre transition stretch and angular distribution in soft biological tissues and cell-seeded hydrogels," *Biomech Model Mechanobiol*, 11(3-4), pp. 325-339.
- [17] Quapp, K. M., and Weiss, J. A., 1998, "Material characterization of human medial collateral ligament," *J Biomech Eng*, 120(6), pp. 757-763.
- [18] Guerin, H. L., and Elliott, D. M., 2007, "Quantifying the contributions of structure to annulus fibrosus mechanical function using a nonlinear, anisotropic, hyperelastic model," *J Orthop Res*, 25(4), pp. 508-516.
- [19] Abraham, A. C., Moyer, J. T., Villegas, D. F., Odegard, G. M., and Haut Donahue, T. L., 2011, "Hyperelastic properties of human meniscal attachments," *J Biomech*, 44(3), pp. 413-418.
- [20] Cortes, D. H., and Elliott, D. M., 2012, "Extra-fibrillar matrix mechanics of annulus fibrosus in tension and compression," *Biomech Model Mechanobiol*, 11(6), pp. 781-790.
- [21] Wagner, D. R., and Lotz, J. C., 2004, "Theoretical model and experimental results for the nonlinear elastic behavior of human annulus fibrosus," *J Orthop Res*, 22(4), pp. 901-909.
- [22] Peng, X. Q., Guo, Z. Y., and Moran, B., 2006, "An anisotropic hyperelastic constitutive model with fiber-matrix shear interaction for the human annulus fibrosus," *Journal of Applied Mechanics*, 73, pp. 815-824.
- [23] O'Connell, G. D., Guerin, H. L., and Elliott, D. M., 2009, "Theoretical and uniaxial experimental evaluation of human annulus fibrosus degeneration," *J Biomech Eng*, 131(11), p. 111007.
- [24] Lake, S. P., Hadi, M. F., Lai, V. K., and Barocas, V. H., 2012, "Mechanics of a Fiber Network Within a Non-Fibrillar Matrix: Model and Comparison with Collagen-Agarose Co-gels," *Ann Biomed Eng*.
- [25] Lake, S. P., and Barocas, V. H., 2011, "Mechanical and structural contribution of non-fibrillar matrix in uniaxial tension: a collagen-agarose co-gel model," *Ann Biomed Eng*, 39(7), pp. 1891-1903.
- [26] Chandran, P. L., and Barocas, V. H., 2006, "Affine versus non-affine fibril kinematics in collagen networks: theoretical studies of network behavior," *J Biomech Eng*, 128(2), pp. 259-270.
- [27] Stylianopoulos, T., and Barocas, V. H., 2007, "Multiscale, structure-based modeling for the elastic mechanical behavior of arterial walls," *J Biomech Eng*, 129(4), pp. 611-618.

- [28] Sander, E. A., Stylianopoulos, T., Tranquillo, R. T., and Barocas, V. H., 2009, "Image-based multiscale modeling predicts tissue-level and network-level fiber reorganization in stretched cell-compacted collagen gels," *Proc Natl Acad Sci USA*, 106(42), pp. 17675-17680.
- [29] Kang, J., Steward, R. L., Kim, Y., Schwartz, R. S., LeDuc, P. R., and Puskar, K. M., 2011, "Response of an actin filament network model under cyclic stretching through a coarse grained Monte Carlo approach," *J Theor Biol*, 274(1), pp. 109-119.
- [30] Nachtrab, S., Kapfer, S. C., Arns, C. H., Madadi, M., Mecke, K., and Schroder-Turk, G. E., 2011, "Morphology and linear-elastic moduli of random network solids," *Adv Mater*, 23(22-23), pp. 2633-2637.
- [31] Stein, A. M., Vader, D. A., Weitz, D. A., and Sander, L. M., 2011, "The micromechanics of three-dimensional collagen-I gels," *Complexity*, 16(4), pp. 22-28.
- [32] Billiar, K. L., and Sacks, M. S., 2000, "Biaxial mechanical properties of the native and glutaraldehyde-treated aortic valve cusp: Part II--A structural constitutive model," *J Biomech Eng*, 122(4), pp. 327-335.
- [33] Holzapfel, G. A., 2000, *Nonlinear Solid Mechanics: A Continuum Approach for Engineering*, John Wiley and Sons.
- [34] Nagel, T., and Kelly, D. J., 2010, "The influence of fiber orientation on the equilibrium properties of neutral and charged biphasic tissues," *J Biomech Eng*, 132(11), p. 114506.
- [35] Benkherourou, M., Rochas, C., Tracqui, P., Tranqui, L., and Gumery, P. Y., 1999, "Standardization of a method for characterizing low-concentration biogels: elastic properties of low-concentration agarose gels," *J Biomech Eng*, 121(2), pp. 184-187.
- [36] Lake, S. P., Hald, E. S., and Barocas, V. H., 2011, "Collagen-agarose co-gels as a model for collagen-matrix interaction in soft tissues subjected to indentation," *J Biomed Mater Res A*, 99(4), pp. 507-515.
- [37] Chandran, P. L., and Barocas, V. H., 2007, "Deterministic material-based averaging theory model of collagen gel micromechanics," *J Biomech Eng*, 129(2), pp. 137-147.
- [38] Stylianopoulos, T., and Barocas, V. H., 2007, "Volume-averaging theory for the study of the mechanics of collagen networks," *Comput Methods Biomech Biomed Engin*, 196(31-32), pp. 2981-2990.
- [39] Weiler, K. J., 1988, "The radial-edge structure: A topological representation for non-manifold geometric boundary representations," *Geometric Modeling for CAD Applications*, M. J. Wozny, H. W. McLaughlin, and J. L. Encarnacao, eds., North, Holland, Amsterdam, pp. 3-36.
- [40] Parasolid web page, "<http://www.ugs.com/products/open/parasolid>."
- [41] Simmetrix web page, "<http://www.simmetrix.com>."
- [42] Shephard, M. S., 2000, "Meshing environment for geometry-based analysis," *Int J Numer Meth Eng*, 47(1-3), pp. 169-190.

Figure Captions

Fig. 1: Computational representations of collagen fiber networks were constructed by randomly placing a set of seed points in a representative volume element, constructing a Voronoi tessellation about these points, defining fibers as the edges of Voronoi elements, removing seed points, and placing pin-joint nodes at each edge-edge and edge-boundary intersection

Fig. 2: Development of the coupled fiber-matrix model: (a) work-flow demonstrating construction protocol for the coupled model; (b) illustration of the conforming multi-dimensional mesh and the mesh classification to the geometric model; (c) schematic showing the interior of the multi-dimensional mesh showing fibers (black lines) and meshed matrix (yellow elements with blue borders)

Fig. 3: (a) Fiber stress, (b) matrix stress, (c) total stress, and (d) RVE Poisson's ratio vs. engineering strain for the coupled fiber-matrix model at varying values of NFM shear modulus; stress values increased with increasing G , particularly for the matrix, while Poisson's ratio decreased (data are representative results from a single network)

Fig 4: Magnitude of stress contributions differed depending on whether simulations were evaluated at constant total strain (solid lines) or constant total stress (dashed lines); (a) while matrix stress values increased in both cases, (b) fiber stresses show opposite trends for the two cases, where decreasing values for the constant-stress case demonstrates stress-shielding (by the matrix) at high shear moduli

Fig. 5: Average (a) matrix stress, (b) fiber stress, and (c) fraction of total stress at 10% strain and with $\nu_{nfm}=0.1$ show good agreement between the parallel and coupled models; stress values at a larger Poisson's ratio (i.e., $\nu_{nfm}=0.45$) at $G=110\text{Pa}$ show a small shift of stress from the matrix to fibers (mean \pm 95%CI; n=5)

Fig. 6: Average (a) fiber stretch, (b) RVE Poisson's ratio, and (c) Ω_{11} (representing fiber orientation in the loading direction) at 10% strain and with $\nu_{nfm}=0.1$ show decreased values for the coupled model compared to the parallel model, but similar qualitative changes as a function of increasing G ; for the case where $\nu_{nfm}=0.1$ and $G=110\text{Pa}$, fiber stretch and Poisson's ratio increased and decreased, respectively, with no change in Ω_{11} ; (mean \pm 95%CI; n=5)

Fig. 7: Interior normal and shear stress fields at 10% strain on the mid-section slice for a representative network ($G=720\text{Pa}$; $\nu_{nfm}=0.1$) demonstrates a highly inhomogeneous distribution for all six independent stress components; slices were cut normal to the loading (1-) direction in the 2-3 plane (represented by the dashed lines in the RVE schematic) and black dots indicate locations where fibers intersect the cutting plane; examples of two regions of high stress concentrations are indicated by arrows in σ_{23} plot

Fig. 8: (a) Maximum and (b) minimum principal stress (normalized by shear modulus of matrix material) distributions at 10% strain over all mesh elements of the matrix material; the mean value increased and the standard deviation decreased as G increased, with curves moving more towards the affine model (values from five networks lumped and plotted)

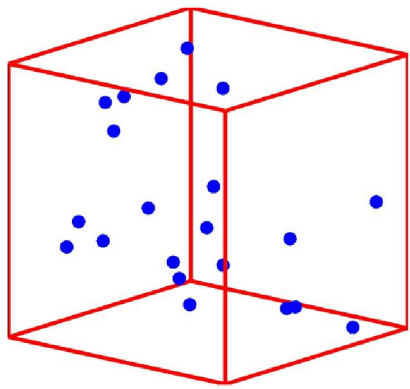
Fig. 9: Distribution of fiber stretch values at 10% strain and with $\nu_{nfm}=0.1$; values concentrated near ~ 1 when G was low (i.e. $G=10\text{Pa}$ and 110Pa), but fibers were stretched

to a greater extent at higher G values, similar to what was shown in the affine model (values from five networks lumped and plotted)

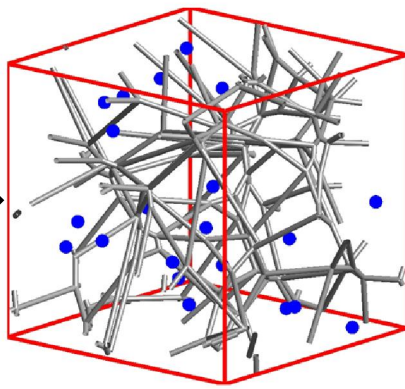
Tables

Table 1: Initial properties of Voronoi networks evaluated in this study.

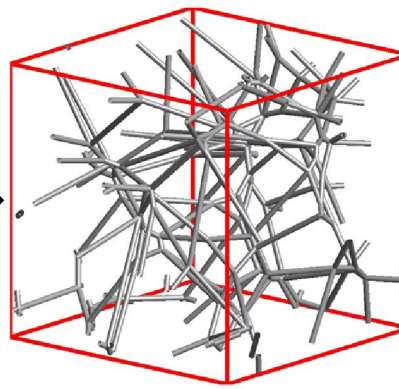
	Number of Fibers	Number of Nodes		Orientation Tensor		
Network	<i>Total</i>	<i>Boundary</i>	<i>Internal</i>	Ω_{11}	Ω_{22}	Ω_{33}
1	689	194	296	0.590	0.196	0.214
2	828	240	354	0.625	0.187	0.188
3	668	196	285	0.607	0.196	0.197
4	725	214	309	0.584	0.198	0.218
5	682	216	287	0.597	0.203	0.200
Mean	718.4	212.0	306.2	0.601	0.196	0.203
Std. Dev.	64.8	18.6	28.3	0.016	0.006	0.012



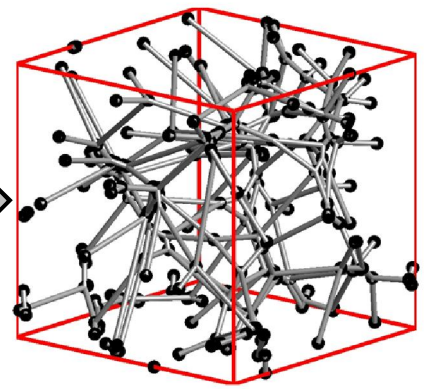
Random Seed Points



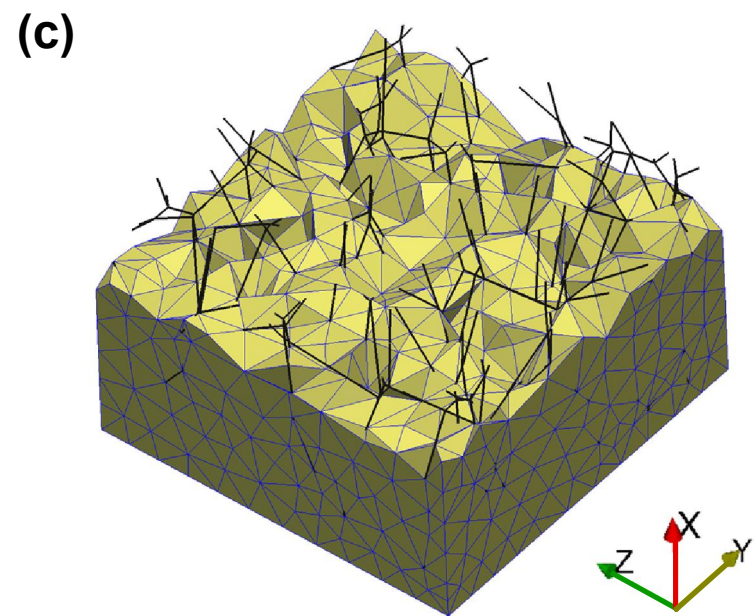
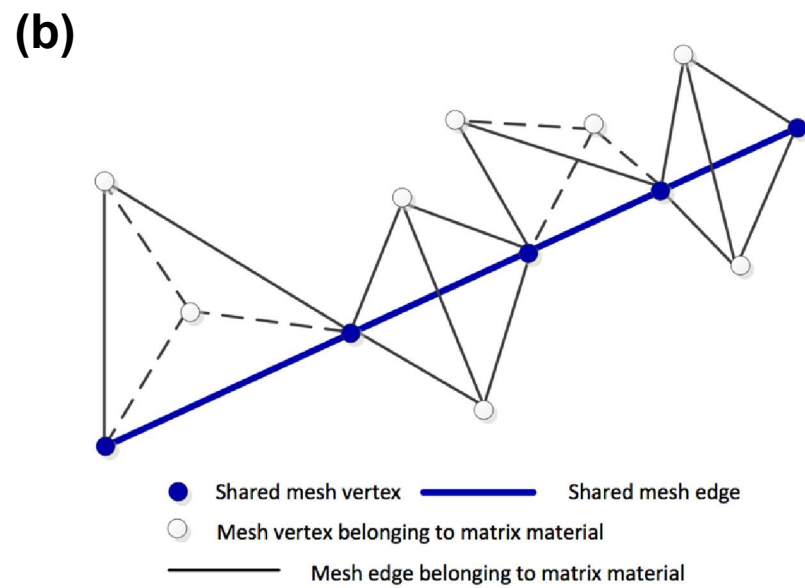
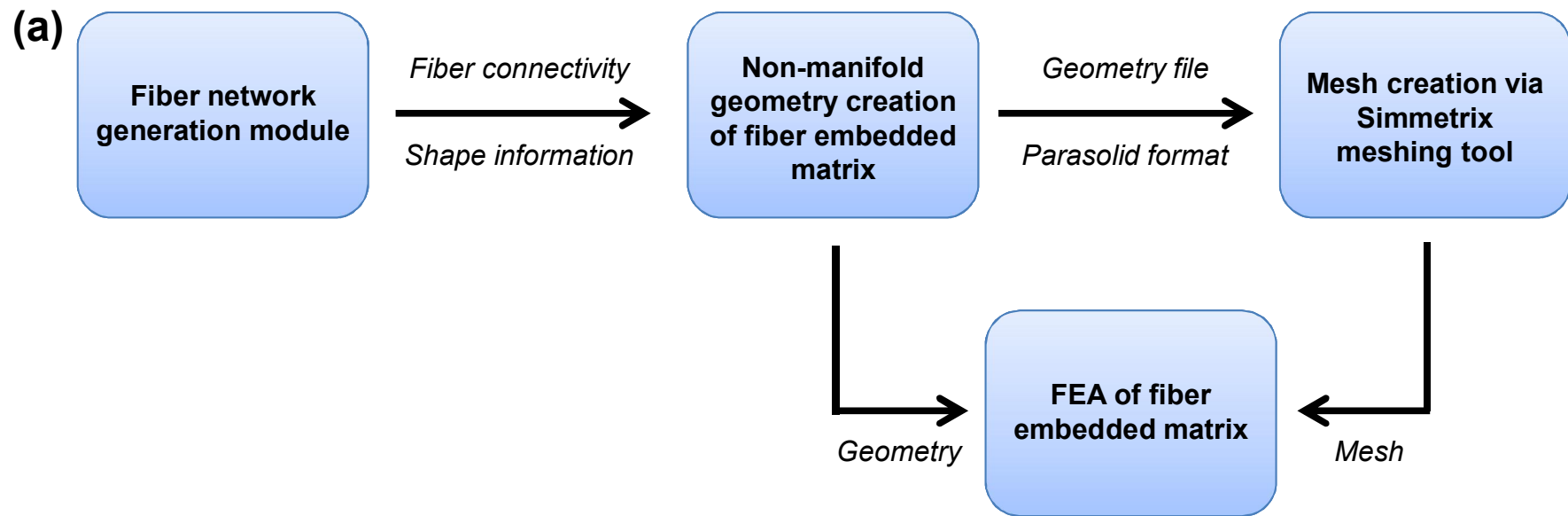
Voronoi Tessellation

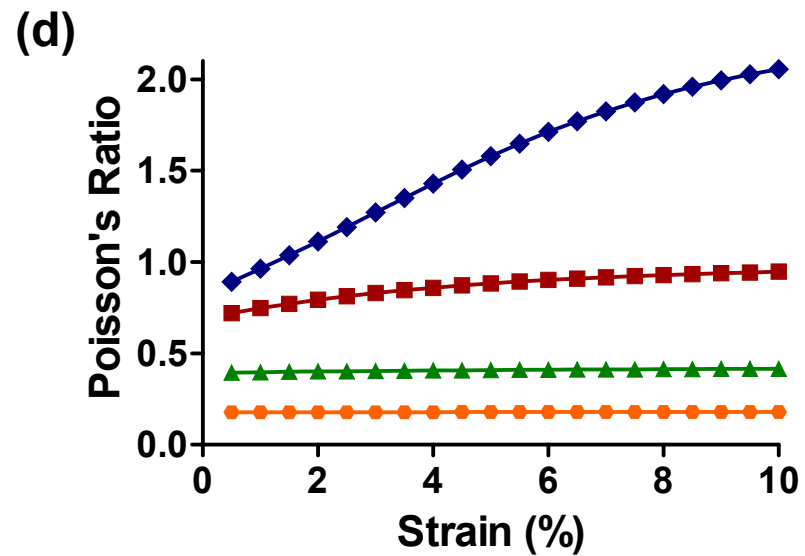
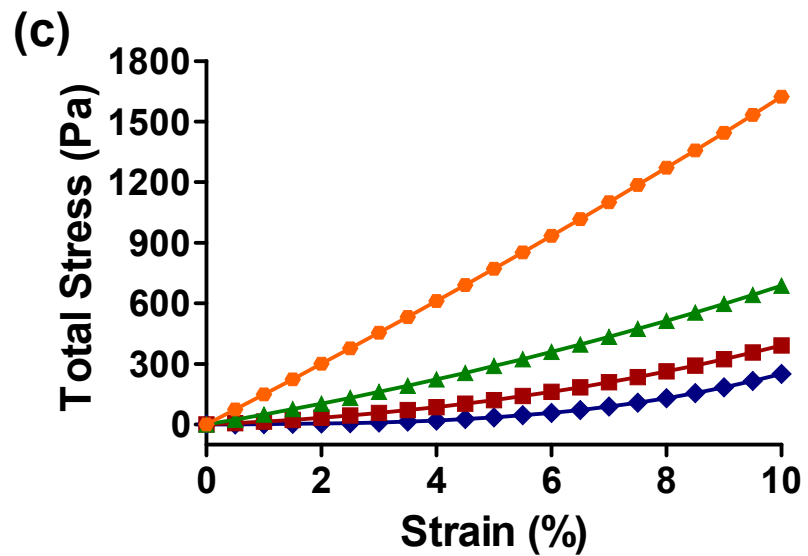
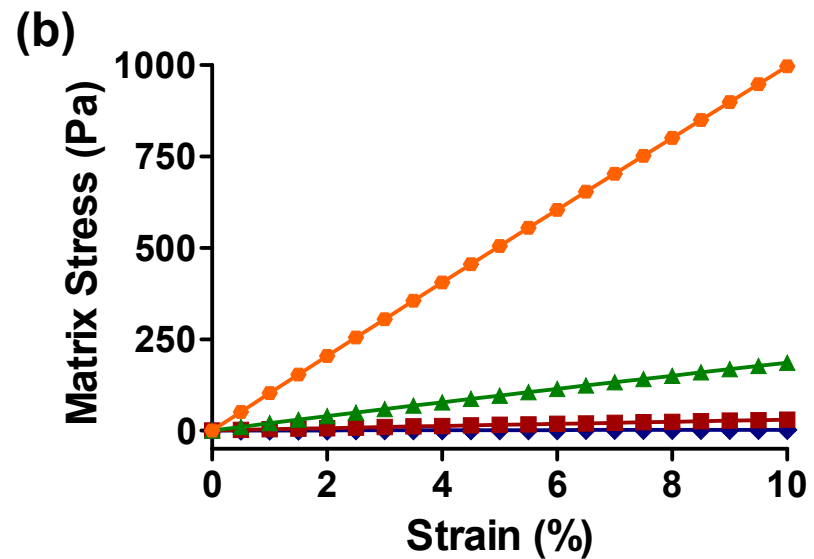
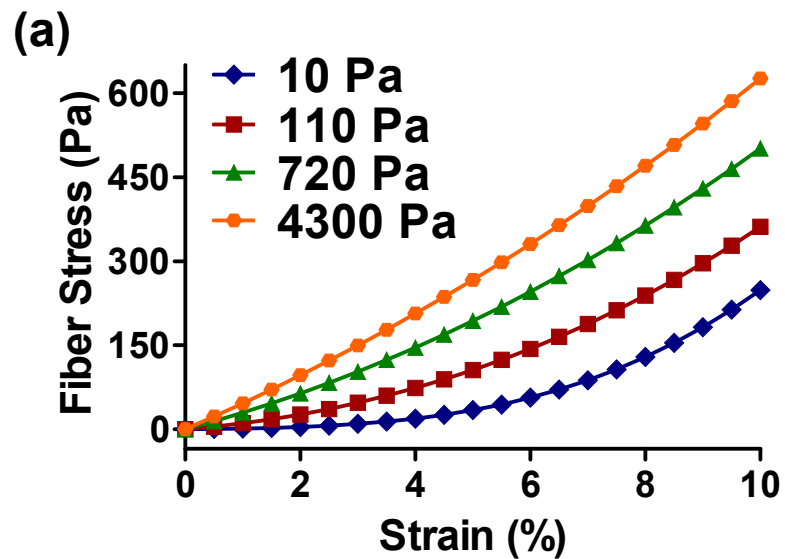


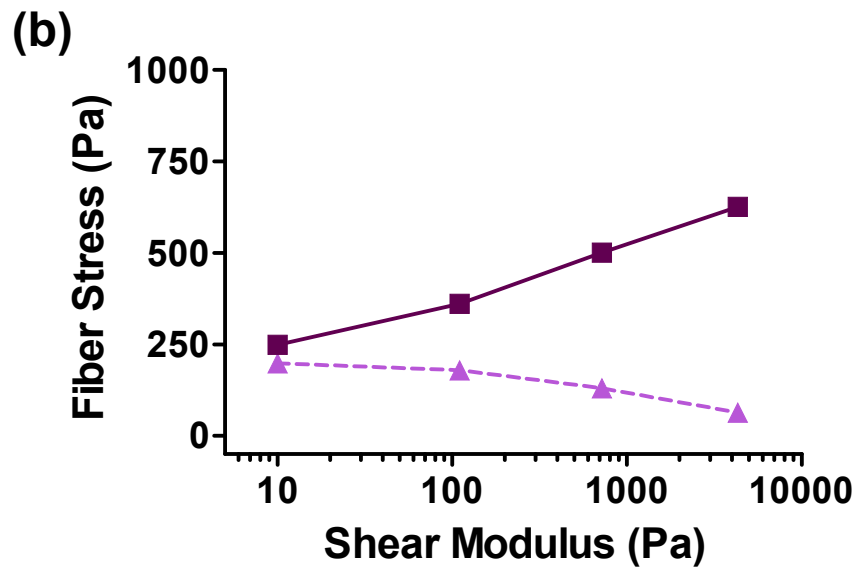
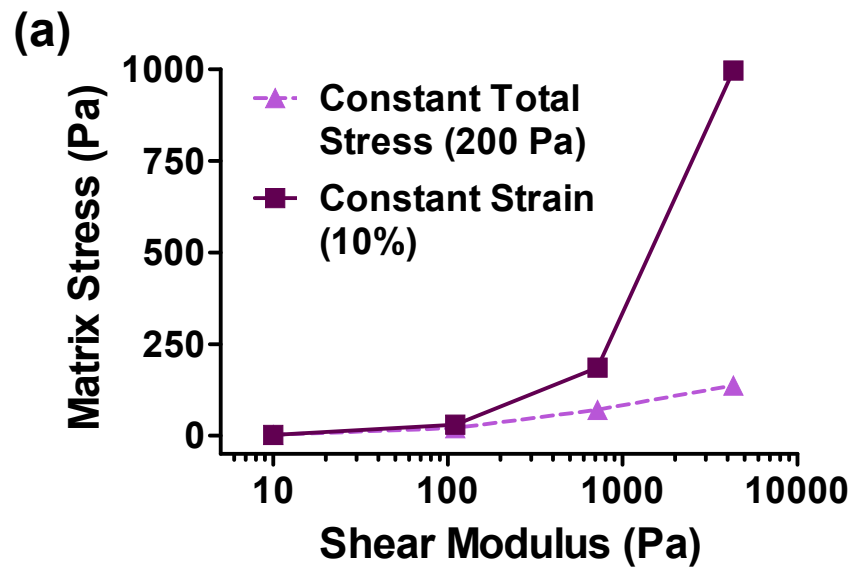
Fiber Network

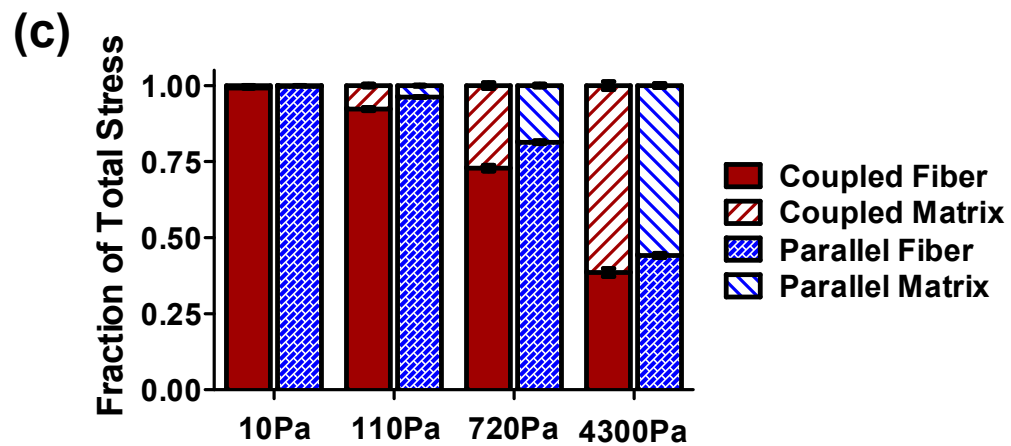
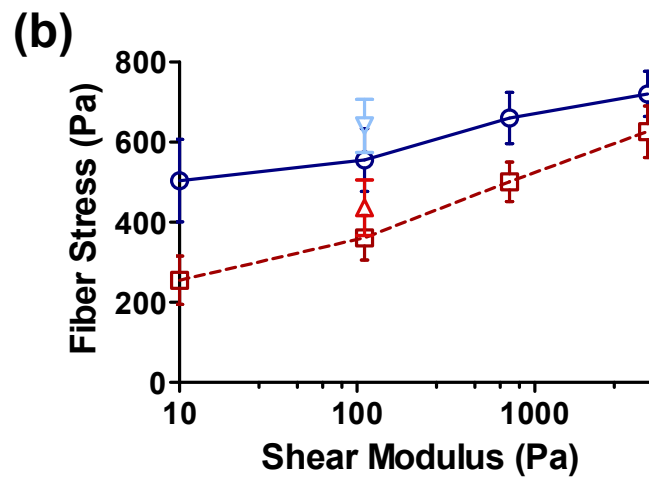
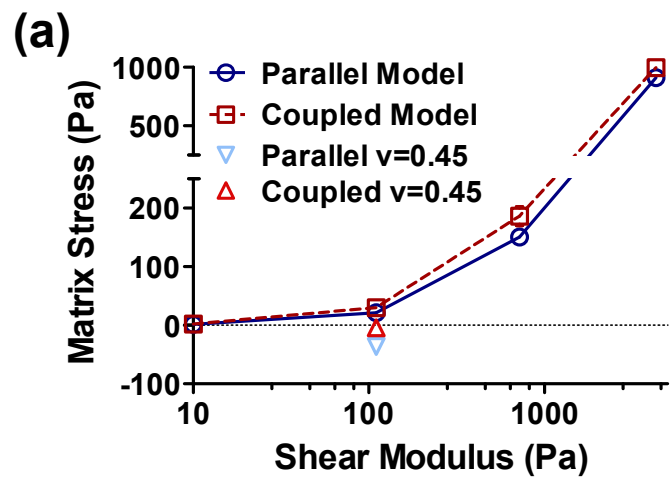


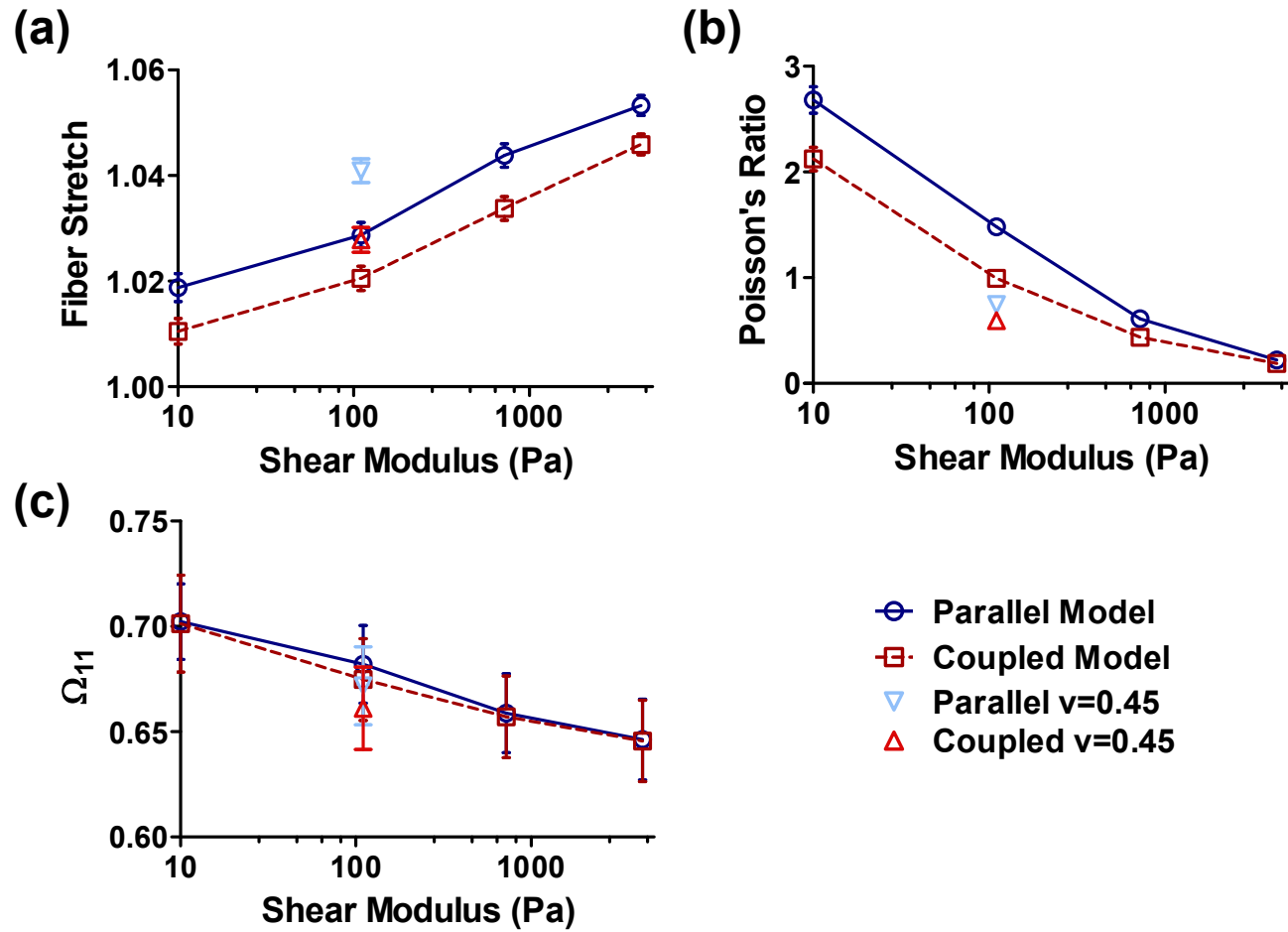
Nodes at Intersections

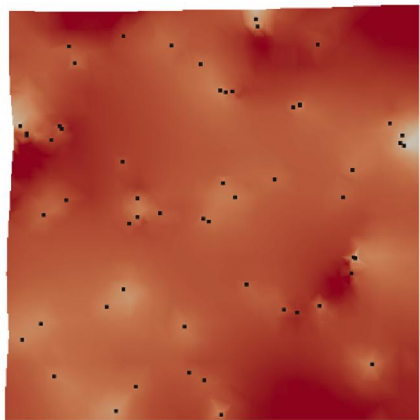




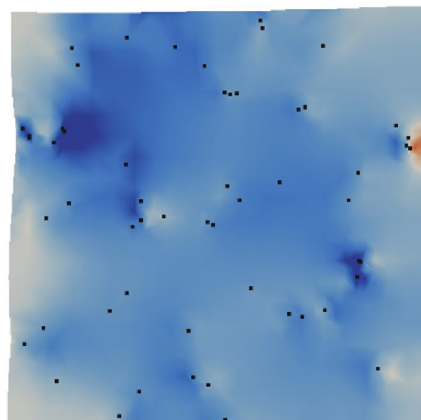




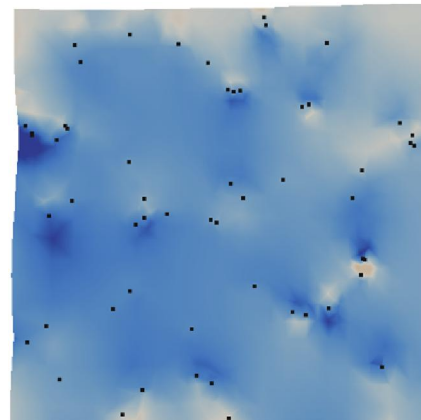




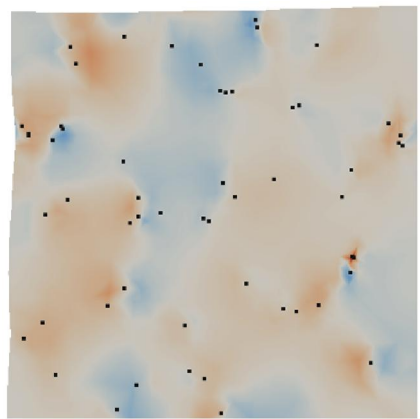
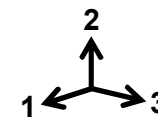
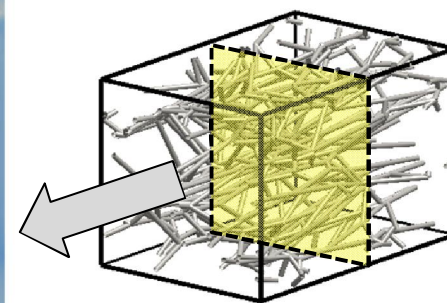
σ_{11}



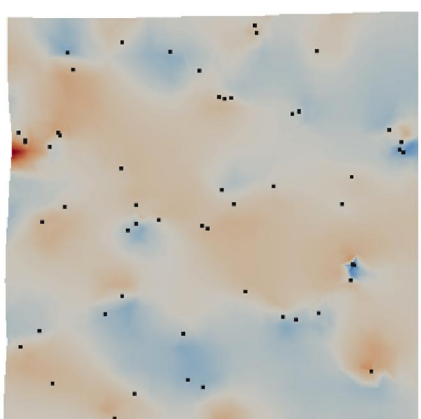
σ_{22}



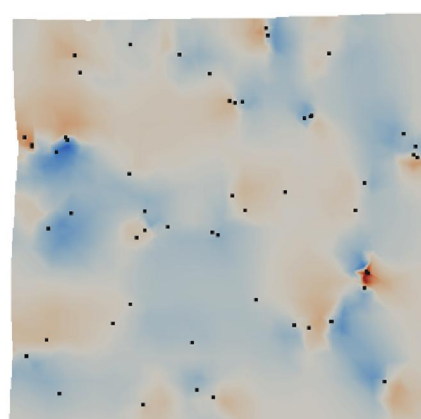
σ_{33}



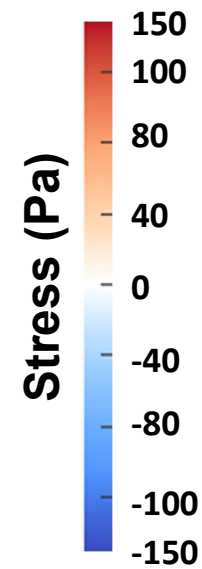
σ_{12}



σ_{13}



σ_{23}



$G=720\text{Pa}$

